ELSEVIER

Contents lists available at ScienceDirect

Journal of Luminescence

journal homepage: www.elsevier.com/locate/jlumin



Integration of near-infrared harvesting transparent luminescent solar concentrators onto arbitrary surfaces



Chenchen Yang^a, Dianyi Liu^a, Alexander Renny^a, Padmanaban S. Kuttipillai^a, Richard R. Lunt^{a,b,*}

- ^a Department of Chemical Engineering and Materials Science, Michigan State University, East Lansing, MI 48824, USA
- ^b Department of Physics and Astronomy, Michigan State University, East Lansing, MI 48824, USA

ARTICLE INFO

Keywords: Luminescent solar concentrator Near-infrared Total internal reflection Transparent photovoltaics Waveguide

ABSTRACT

Visibly transparent luminescent solar concentrators (TLSCs) can convert existing window glazing systems and non-window surfaces into solar energy harvesting resources, dramatically improving energy utilization efficiency. While there has been a significant interest in improving the power conversion efficiency, little attention has been focused on the challenges of integrating luminescent solar concentrators (LSCs) onto non-window surfaces or windows with significant infrared absorption coefficients. In these situations, the total internal reflection (TIR) can be effectively disabled when LSCs are directly and seamlessly integrated onto surfaces that are highly absorptive or scattering to infrared light. To overcome this challenge, we utilize a low refractive index adhesive film with high transparency between the TLSC waveguide and the back surface, to maintain both the device functionality and aesthetic quality of the surface underneath. Photovoltaic measurements were conducted to show that the TIR is re-enabled with the presence of such a structure. Thus, this method can effectively improve LSC performance and scalability, and allows TLSCs to be integrated onto arbitrary surfaces such as automobiles, billboards, and buildings.

1. Introduction

Seamless installation of solar harvesting systems [1] onto areas provide a practical approach to utilize renewable solar energy more efficiently over currently existing surfaces [2–5]. This includes surfaces such as windows and skylights but also surfaces where the underlying aesthetics are important such as billboards, building exteriors, colorful cars, and signage. Transparent luminescent solar concentrators (TLSCs) are one example of a technology that has been designed to exploit surfaces for solar harvesting that can offer high defect tolerance, mechanical flexibility, angle independence, and low cost [6]. TLSCs selectively harvest the invisible portion of the incident solar flux (ultraviolet (UV) or near-infrared (NIR)) and allow the visible light to pass through, which minimizes the visual impact and enables the adoption in areas previously inaccessible [7,8]. Thus, TLSCs are a very promising candidate to supply the energy demand of currently existing surfaces on-site

Various luminophores have been applied to luminescent solar concentrators (transparent and opaque), including quantum dots [9-16], rare-earth ions [17-25], nanoclusters [8,11,26,27] and organic molecules [7,28-34]. Most of these reports focus on the improvement of quantum yield (QY) [35-37] and the modulation of the absorption and

emission spectra of the luminophores to increase the Stokes shift [8,38-40] or to match the absorption peak of the luminophore with the peak of the incident solar spectrum [41-43] with the aim to enhance the photovoltaic performance of the LSC device as well as the scalability [6]. Fig. 1 illustrates the operating principles of a TLSC system: the invisible portion of the solar spectrum is absorbed by luminophores embedded in a transparent waveguide. That absorbed solar energy is then re-emitted within the waveguide at an invisible (i.e. infrared) wavelength. Due to the difference of refractive index between the waveguide and the ambient environment the re-emitted photons are predominantly trapped within the waveguide by total internal reflection (TIR), directing them towards the waveguide edges where these reemitted photons can be converted into electrical power in photovoltaic cells. According to Snell's law, the key to ensuring TIR is that the waveguide is made of a material with higher index of refraction (n) value than that of both the front and back claddings [5,6]. The waveguide material should also have low extinction coefficient (k) or scattering coefficient at the wavelength range of the photoluminescence. Such an example is shown in Fig. 1 where the windshield glass of a car $(n_{glass} \cong 1.50)$ in contact with air $(n_{air} = 1.0)$ on both sides can function effectively as a waveguide for TLSCs. However, when a TLSC is integrated onto arbitrary surfaces such as the siding of a car, the back of

E-mail address: rlunt@msu.edu (R.R. Lunt).

^{*} Corresponding author.

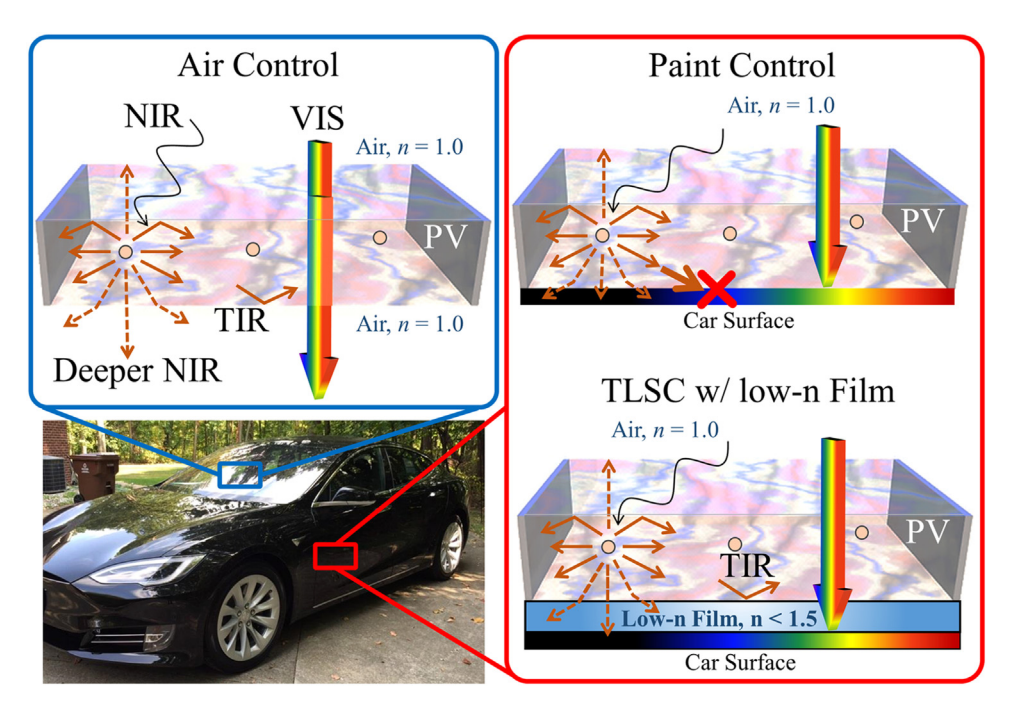


Fig. 1. Conceptual schematic showing a near-infrared (NIR) harvesting transparent luminescent solar concentrator (TLSC) integrated onto the window ("Air Control") and non-window ("TLSC w/ Low-n Film") parts of an automobile. While a black automobile is pictured, this could be applied to any color automobile without changing the architecture. With direct integration of LSC and TLSCs on such surfaces (included in the schematic as "Paint Control") total internal reflection (TIR) is lost.

the waveguide is no longer in contact with air but seamlessly adhered with the solid surface beneath. This results in re-emitted photons entering the back surface and being lost to absorption or scattering from that surface. Spacing an air gap between the waveguide and the surface underneath can regain this waveguide function, however, air gaps generally lack structural stability rendering them unsuitable for robust applications.

In this work, we demonstrate a route to enable the performance of TLSC devices as they are installed onto arbitrary surfaces. We have developed an optical approach to confine the TIR to the optically transparent waveguide and prevent surface absorption that can effectively turn off the TLSC device. Conceptually, a neat layer with a low refractive index is coated onto the back side of the TLSC to function as cladding and adhesive for the waveguide (Fig. 1). NIR-selective harvesting organic dye/polymer host composite is then coated onto the front surface of the waveguide as the luminophore film. Due to the NIRabsorption of the organic dye combined with visible/infrared transparency of the low refractive index film, the overall visual impact of the whole TLSC device is minimized while the functionality and aesthetic quality of the surface underneath are largely unaffected. Both the current density-voltage (J-V) characteristics and distance-dependent external quantum efficiency (EQE) measurements show that the insertion of the low refractive index film can effectively re-enable the LSC device and substantially improve the power conversion efficiency (PCE) and scalability in comparison to the TLSC control devices without such an approach. This design provides a simple and scalable method to resolve the challenge of seamless integration of TLSCs onto any surface to help realize the full potential of LSC and TLSC devices beyond windows.

2. Experimental

2.1. Module fabrication

"Air Control" TLSC: $200 \, \mathrm{mg} \, \mathrm{L}^{-1}$ 1-(5-carboxypentyl)-3,3-dimethyl-2-((*E*)-2-((*E*)-3((*E*)-2-(1,3,3-trimethylindolin-2ylidene)ethylidene)cyclohex-1-enyl)vinyl)-3*H*-indolium chloride (Cy7-CA) (Lumiprobe) ethanol solution was mixed with mounting medium (Fluoroshield F6182, Sigma-Aldrich) at a volume ratio of 1:2. This mixture was dropcast on the front surface of a 5.08 cm \times 5.08 cm \times 0.635 cm glass sheet (for photovoltaic characterization) and allowed to dry for 6 h in a glove-

box filled with nitrogen gas (O_2 , $H_2O < 1$ ppm), resulting in a layer thickness of 0.5 mm. Dichloromethane was mixed with (poly)-butyl methacrylate-co-methyl methacrylate (PBMMA) (Sigma-Aldrich) at a volume ratio of 1:1. This mixture was then drop-cast onto the dye/ waveguide composite film to make a smooth and flat surface to avoid light scattering in the waveguide and act as a protection layer. The same layer structure was applied for $2.54\,\mathrm{cm}\times2.54\,\mathrm{cm}\times0.1\,\mathrm{cm}$ (for photoluminescence (PL) measurements) or $1.27 \text{ cm} \times 1.27 \text{ cm} \times 0.07$ cm (for QY measurements). For photovoltaic measurements, singlecrystalline solar cells (Vikocell) were laser cut into $5.08\,\mathrm{cm}\times0.635\,\mathrm{cm}$ strips for PCE and corresponding EQE measurements and 10.16 cm \times 0.635 cm strips for normalized position-dependent *EQE* measurements. For PCE measurements, two PV strips were mounted on orthogonal edges using index matching gel (Thorlabs) to attach the PV strips on glass edges and were connected in parallel. Each device was tested with the same PV cells. The remaining two edges were covered with specular film reflector (DF2000MA series, 3 M). For EQE measurements, one PV strip was attached to one edge of the waveguide with the other three edges painted black.

Thin, low index polymer layers were coated onto the backside of the waveguide sheet by doctor blade, and the thickness of these low refractive index films ("n=1.30" or "n=1.38", MY Polymers) are controlled to 0.5 mm. A PBMMA film was then formed on top of the low refractive index layer as a polymer protection film by drop-casting. This PBMMA film is necessary for good adherence of the following paint layer and to protect the previously coated low index layers from redissolution. After the PBMMA film is dried, paint is sprayed uniformly to form a dense and smooth paint film. The front surfaces and edges of "n=1.30", "n=1.38" and "Paint Control" TLSCs are the same as the "Air Control" TLSC.

2.2. Optical characterization

Specular transmittance of both solutions and films were measured using a dual-beam Lambda 800 UV/VIS spectrometer in the transmission mode. The PL for Cy7-CA in both solutions and polymer films were measured by using a PTI QuantaMaster 40 spectrofluorometer with excitation at 675 nm. Quantum yield measurements were tested by using Hamamatsu Quantaurus fluorometer, excitation ranges in scan mode (10 nm per scan step) were adjusted to 700–750 nm for Cy7-CA.

Six *QY* values were collected, and the reported *QY* was averaged from these six *QY* values with corresponding excitation wavelengths.

2.3. Module photovoltaic characterization

J-V measurements were obtained using a Keithley 2420 source measurement under simulated AM1.5G solar illumination (xenon arc lamp with the spectral-mismatch factor of 0.97 \pm 0.03 for all the devices tested). The light intensity was calibrated with an NREL-calibrated Si reference cell with KG5 filter. For position-dependent EQE measurements, the excitation beam was obtained by directing chopped incident light from a quartz tungsten halogen lamp through a monochromator. EOE scans were performed by positioning the monochromatic excitation beam from a fiber perpendicular to the LSC waveguide front surface at various distances from a single edge-mounted Si PV cell. The measured EQE was corrected by the geometric factor, $g = \pi/tan^{-1}(L/2d)$, which accounts for the different angle subtended by the solar cell at various distance *d*, where *L* is the LSC plate length. Note both PCE and EQE measurements were tested by using the same TLSC to match the J_{SC} with the integrated J_{SC} , and a matte black background was placed on the back of the tested TLSC device to eliminate the illumination from the environment or reflection (double pass) for both PCE and EQE measurements. We also utilize the same PV cells mounted around the edge to eliminate any PV-to-PV variations in performance.

2.4. Optical modeling

In considering reabsorption losses from the overlap in the absolute absorption and normalized emission spectra, the optical efficiency $\eta_{opt}(\lambda)$ of the "Air Control" TLSC system was numerically evaluated in Matlab as a function of distance d, plate length L, plate thickness t_0 and dye/polymer film thickness t. The complete equations used in this simulation can be found in our previous work [6].

3. Results

Cyanine dye Cy7-CA is used as the NIR-selective harvesting luminophore for all the TLSC devices. The molecular structure of Cy7-CA is shown in Fig. 2a, and the absorption/emission spectra in both dichloromethane (DCM) solution and in polymer matrix are plotted in Fig. 2b. The absorption and photoluminescence spectra of the Cy7-CA in polymer matrix and in DCM solution are very close to each other: the absorption spectra peak at 760 nm for DCM solution and 762 nm for dye/polymer composite film, while the NIR emission peaks are 787 nm for DCM solution and 788 nm for dye/polymer composite film. The photoluminescent quantum yield (QY) is 24 \pm 1 in DCM solution and 19 \pm 1 in polymer matrix.

TLSC devices are formed on borosilicate glass sheets with an active area of 25.8 cm². To demonstrate the principle of this design, cyanine dye molecules are dissolved in ethanol, mixed with a polymer host, and then drop-cast onto glass sheets to form dye/polymer composite films. Laser-cut Si photovoltaic cells are mounted around the two orthogonal edges and connected in parallel and the other two orthogonal edges are taped with reflective films (see Section 2 for details). TLSC devices with four different layer structures (as shown in Fig. 1) are made and their photovoltaic characteristics are compared. We utilize two different commercially available low index polymers (n = 1.30 and n = 1.38) to compare to an air control (air as the claddings on both sides of the waveguide) and a paint control (just a paint layer on the back surface of the waveguide). The current density versus voltage (J-V) characteristics of these TLSCs are shown in Fig. 2c along with the absolute position dependent external quantum efficiency (EQE) of the air-control in Fig. 2d and the relative EQEs for the other configurations in Fig. 3. The measured short-circuit current density (JSC) of the device with Cy7-CA is $1.11 \pm 0.02 \,\mathrm{mA\,cm^{-2}}$, with an open-circuit voltage (V_{OC}) of $0.47 \pm 0.01 \, \text{V}$ and a fill factor (FF%) of 55 \pm 1%, leading to an efficiency (0.30 ± 0.01%) similar to previous reported Cy7-CA device considering the larger area tested here (devices with a smaller area of 4 cm^2 shown a *PCE* of 0.40 \pm 0.03%). In contrast to the "Air Control" TLSC, the "Paint Control" TLSC exhibits a very poor photovoltaic behavior, which shows a J_{SC} of 0.31 \pm 0.02 mA cm⁻², V_{OC} of 0.38 \pm 0.01 V, FF% of 54 \pm 1%, and a PCE of only 0.07 \pm 0.01%. When we integrate the low-index polymers, "n = 1.30" and "n = 1.38", into the TLSC devices, the corresponding PCE is improved to 0.21 \pm 0.03% and 0.16 \pm 0.01%, with J_{SC} of 0.82 \pm 0.09 mA cm⁻² and 0.62 \pm 0.02 mA cm⁻², V_{OC} of 0.46 \pm 0.01 V and 0.43 \pm 0.01 V, and FF% of 56 \pm 1% and 55 \pm 1%, respectively. Thus, adding these low refractive index films significantly restore their photovoltaic performance compared to the "Paint Control". Fig. 2d shows the EOE spectra of the "Air Control" TLSC as a function of excitation position (see Section 2 for details of the measurements). The EQE peak position of the TLSC (i.e. at 760 nm) matches the absorption spectrum of Cy7-CA in polymer matrix in Fig. 2b and no direct excitation of the edge mounted solar cell is observed in any of the EQE spectra. The calculated photocurrent density from integrating the product of the EQE and AM 1.5G solar spectra is 0.91 mA cm⁻² of the "Air Control" TLSC, which is in good agreement with the J_{SC} extracted from J-V measurements.

These data show that the presence of the low refractive index film imparts minimal visual impact such as absorptive coloring or tinting. The transmission spectra of the low refractive index films are compared with that of waveguide alone in Fig. 2e. The transmission spectrum curves of both the "n = 1.30" and "n = 1.38" films on the waveguide sheets nearly overlap with that of the waveguide alone across the whole visible spectrum (from 400 nm to 900 nm), so the corresponding average visible transmittance (AVT) and color rendering index (CRI) for "n = 1.30" is 91.3% and 99.8, respectively [2,3,6]. For "n = 1.38", the AVT is 90.6% and CRI is 99.0 compared to 92.2% and 100 for the waveguide alone, respectively. The transmission spectrum of the paint film is also included in the same plot, which indicates that the paint film completely blocks the entire incident light from 300 nm to 900 nm. To check the validity of photon balance from the independent EQE, transmission $(T(\lambda))$, and reflection $(R(\lambda))$ spectra measurements of the "Air Control" TLSC device, we show that $EQE(\lambda)+R(\lambda)+T(\lambda) \le 1$ is satisfied at each wavelength in Fig. 2f [3]. The transmission spectrum of the "Air Control" TLSC device has a corresponding AVT of 87.7% and CRI of 92.3. For the majority of window and glazing system applications, a device should have AVT > 65-75% and CRI > 90, and therefore the "Air Control" TLSC with Cy7-CA is well suited for this requirement. Although there is not a similar standard for transparent PVs applied to non-transparent surfaces, higher AVT and CRI will always lead to better color fidelity (quantitatively, for example, with CIE chromaticity coordinates) of the original aesthetic quality of the back surfaces, which is critical in many applications and particularly important for automobiles.

To explore the impact of the low refractive index film on device scalability, TLSC systems with the four different structures were characterized by position-dependent EQE as a function of the distance (d) from the excitation source to the same edge-mounted PV cell. Multiple EQE scans were taken for each TLSC system as d was increased from 15 mm to 95 mm (10 mm interval). The EQE spectra of the TLSC devices with four different layer structures are plotted in Fig. 3a-d and the EQE peak values of each individual scan were extracted and plotted in Fig. 4a.

4. Discussion

The wavelength-dependent EQE of an LSC $(EQE_{LSC}(\lambda))$ can be expressed as:

$$EQE_{LSC}(\lambda) = \eta_{opt}(\lambda) \cdot \frac{\int EQE_{PV}(\lambda')PL(\lambda')d\lambda'}{\int PL(\lambda')d\lambda'}$$
(1)

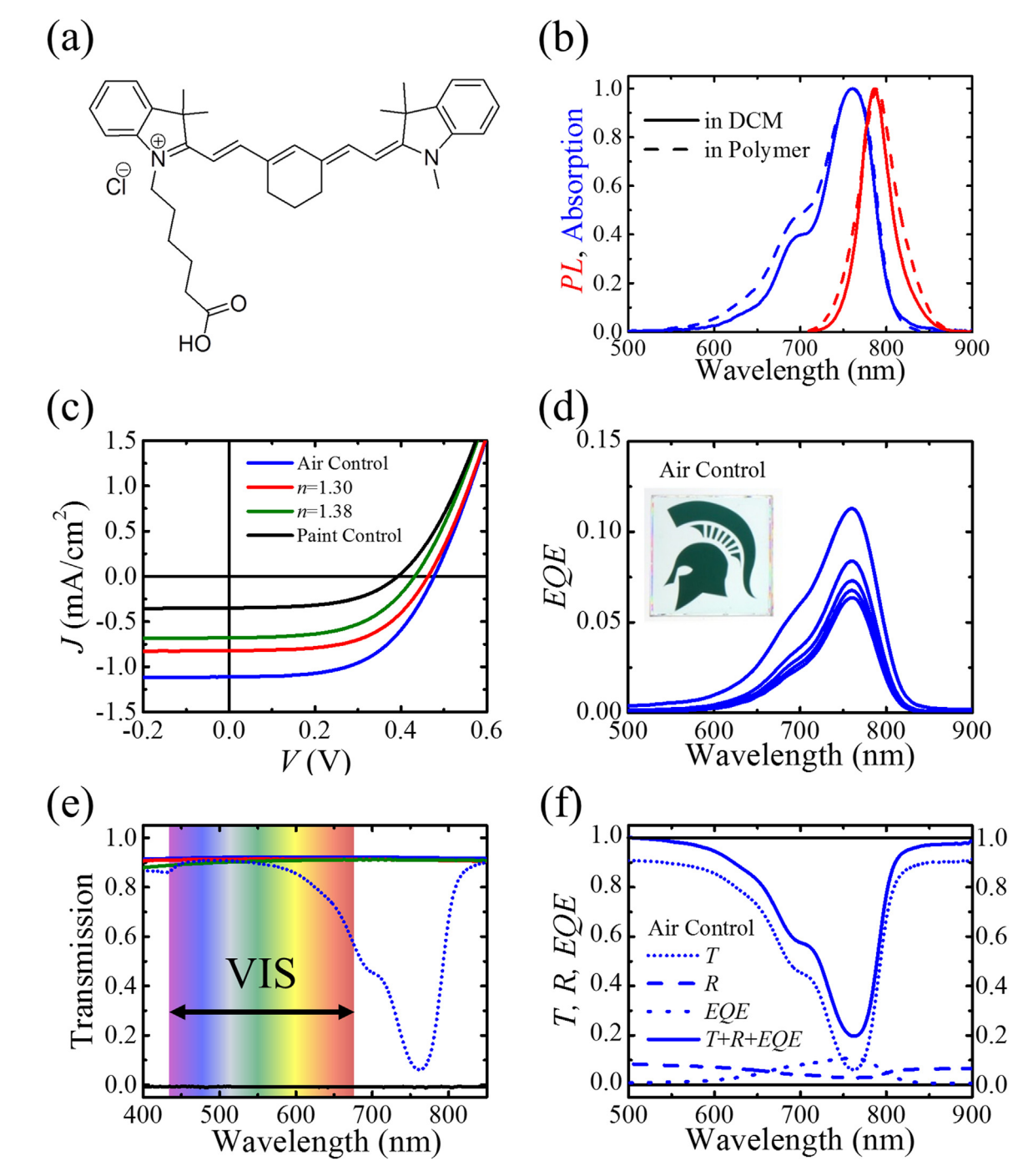


Fig. 2. (a) The molecular structure of Cy7-CA. (b) Normalized absorption (blue) and emission spectra (red) of Cy7-CA in DCM solution (solid lines) and polymer matrix film (dashed lines). (c) Current density as a function of voltage (J-V curves) for the fully assembled TLSC systems with different layer structures including "Air Control" (blue), "n = 1.30" (red), "n = 1.38" (olive) and "Paint Control" (black). (d) Absolute external quantum efficiency (EQE) of "Air Control" TLSC system as a function of wavelength (measured at d = 5 mm, 15 mm, 25 mm, 35 mm and 45 mm), inset: photograph of "Air Control" TLSC. (e) Transmission spectra for waveguide alone (blue, solid), "n = 1.30" film coated on the backside of the waveguide (green, solid), paint on the backside of the waveguide (black, solid) and "Air Control" TLSC device (blue, short dot). Average Visible Transmittance (AVT) and Color Rendering Index (CRI) were calculated based on these transmission spectra. (f) Transmission ($T(\lambda)$), reflection ($R(\lambda)$), EQE, and photon balance ($EQE(\lambda) + R(\lambda) + T(\lambda)$) ≤ 1 of the "Air Control" TLSC device.

where $\eta_{opt}(\lambda)$ is the LSC optical efficiency (number of photons emitted at the edge per number of photons incident) at the absorption wavelength of the luminophore and the integral represents the *EQE* of the edge-mounted PV cell over the emission wavelengths of the luminophore. To avoid confusion, it should be noted that the integrals here are performed over the wavelength range of the *PL* emission (λ') not the wavelength of the incident light (λ). In the emission wavelength range

Cy7-CA (700–850 nm) the edge-mounted Si PV show a nearly constant EQE (~90%) so that Eq. (1) simplifies to $EQE_{LSC}(\lambda) = \eta_{opt}(\lambda) \cdot EQE_{PV}$, where $EQE_{PV} \cong 0.90$. The optical efficiency at a specific wavelength can be further expanded into the product of five loss factors:[6]

$$\eta_{opt}(\lambda) = (1 - R_f(\lambda)) \cdot A(\lambda) \cdot \eta_{PL} \cdot \eta_{Trap} \cdot \eta_{RA}$$
(2)

where $R_f(\lambda)$ is the reflection spectrum of the incident light at the front

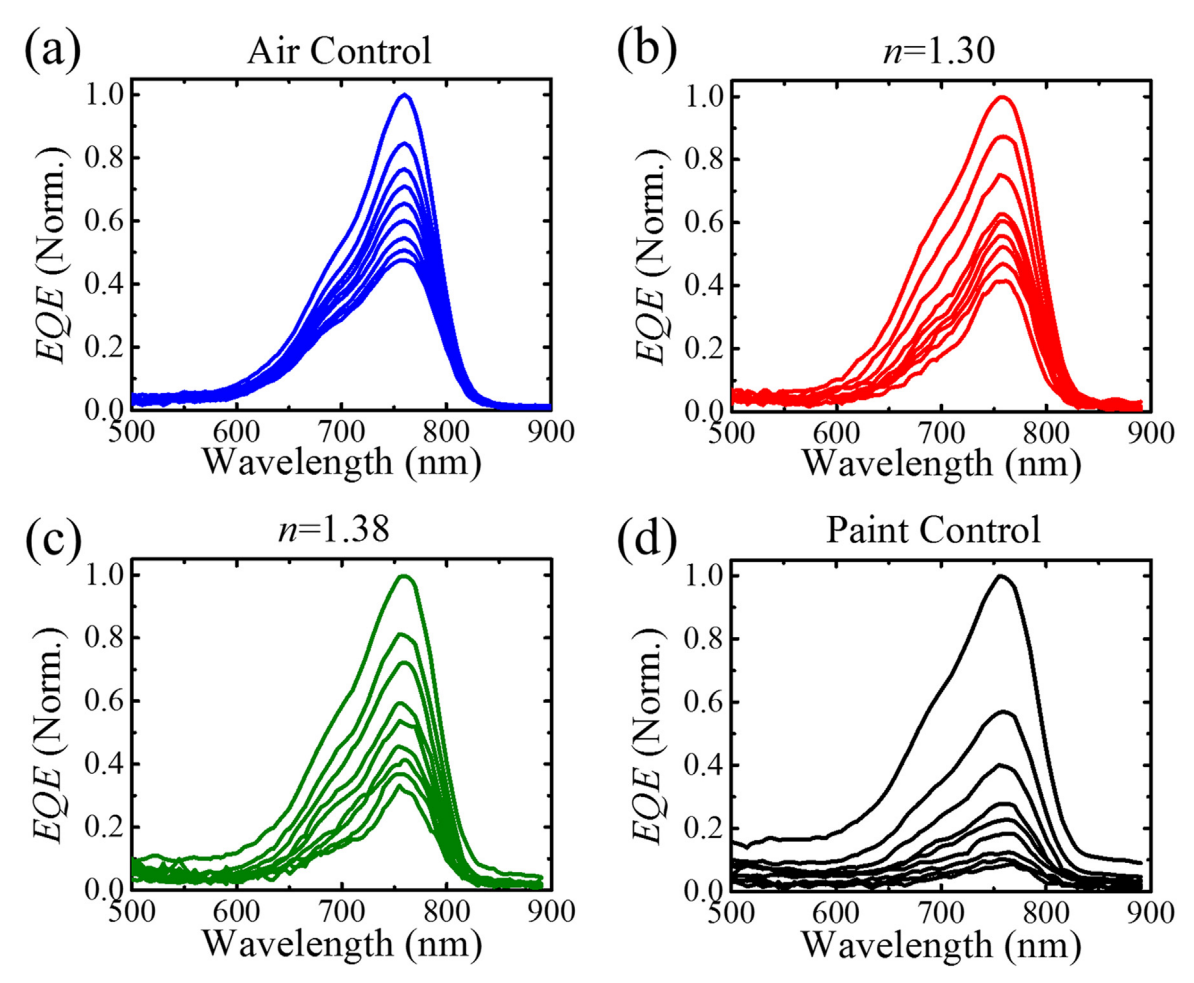


Fig. 3. Position-dependent EQE of "Air Control" (a), "n = 1.30" (b), "n = 1.38" (c) and "Paint Control" (d) as a function of wavelength measured from 15 mm to 95 mm, with 10 mm increments.

surface so the term $(1-R_f(\lambda))$ is the portion of incident solar flux entering the TLSC device without being reflected, $A(\lambda)$ is the normal incidence absolute absorption at a given wavelength (calculated by $A(\lambda)=1-R(\lambda)-T(\lambda)$), η_{PL} is the luminescence efficiency of the luminophore (the QY of the luminophore in polymer matrix), η_{Trap} is the photon trapping (or waveguiding) efficiency, and η_{RA} is the efficiency of suppressing reabsorption. For comparison to other literature reports, the internal quantum yield or internal optical efficiency $(\eta_{lopt}(\lambda))$ which is the number of photons emitted at the edge per number of photons absorbed is also calculated as:

$$\eta_{lopt}(\lambda) = \frac{\eta_{opt}(\lambda)}{A(\lambda)} = \frac{EQE_{LSC}(\lambda)}{EQE_{PV} \cdot A(\lambda)}$$
(3)

 $\eta_{iopt}(\lambda)$ of an LSC device is constrained by the corresponding QY of the luminophore in the polymer matrix, the difference is that $\eta_{iopt}(\lambda)$ accounts for waveguiding and reabsorption losses. For the "Air Control" TLSC, the peak internal quantum yield $(\eta_{iopt}(\lambda=760nm))$ is 13.6% at d=5 mm and 7.7% at d=45 mm, and the overall η_{iopt} across the absorption spectra (600–800 nm) is relatively constant between 12% and 14% at d=5 mm and 5–8% at d=45 mm.

Since all four TLSC devices possess the same polymer encapsulation film, dye/polymer matrix film and waveguide, these loss factors $((1-R_f(\lambda)),A(\lambda),\eta_{PL})$ are essentially independent of the low refractive index film. For simple waveguides, the trapping efficiency (η_{Trap}) is a function of the refractive index of the waveguide cladding: $\eta_{Trap}=\sqrt{1-n_{cladding}^2/n_{waveguide}^2}$. As for the case of the waveguide having two claddings with different refractive index values, η_{Trap} is dominated by the cladding side with lower refractive index due to its larger critical

angle (θ_C) for TIR at the waveguide/cladding interface. The reabsorption efficiency η_{RA} is a function of both η_{Trap} and η_{PL} , but it is weakly dependent on the refractive index of the waveguide and cladding compared to η_{Trap} itself. Thus, the difference in $EQE_{LSC}(\lambda)$ roll-off behavior should be dominated by η_{Trap} .

As shown in Fig. 4a the "Air Control" TLSC has the highest trapping efficiency so the EQE decay trend is the slowest since it has both front and back surfaces in contact with air. Once the backside of the waveguide is configured with an absorptive paint film the TIR is no longer confined within the waveguide and the light penetrates into the paint layer. This results in the parasitic absorption and scattering of the light from the paint layer that leads to rapid EQE decays for the "Paint Control" and a factor of 4 lower PCE. Some remaining EQE signal can still be collected at very short distances (small d) as shown in Fig. 3d which is mainly from a very small portion of the emitted photon flux reaching the edge-mounted PV directly through the waveguide but not via TIR. This explains why some residual short-circuit current density can still be detected from the J-V measurement for the corresponding TLSC device in Fig. 2c. This straight-through luminescent is strongly sensitive to the waveguide thickness, where there is a smaller emission angle range for photons to reach the edge as the waveguide thickness decreases or the length of the device increases. Nonetheless, the PCE is reduced by nearly 75% even for devices of 5 cm length and would be an even greater loss as the device size is increased.

We also fabricated "Paint Control" TLSC devices with different colors (blue, green, red and white) to mimic the arbitrary back surfaces and extracted their EQE peak values as a function of d and plotted in Fig. 4b. All the colored "Paint Control" TLSCs show very similar EQE

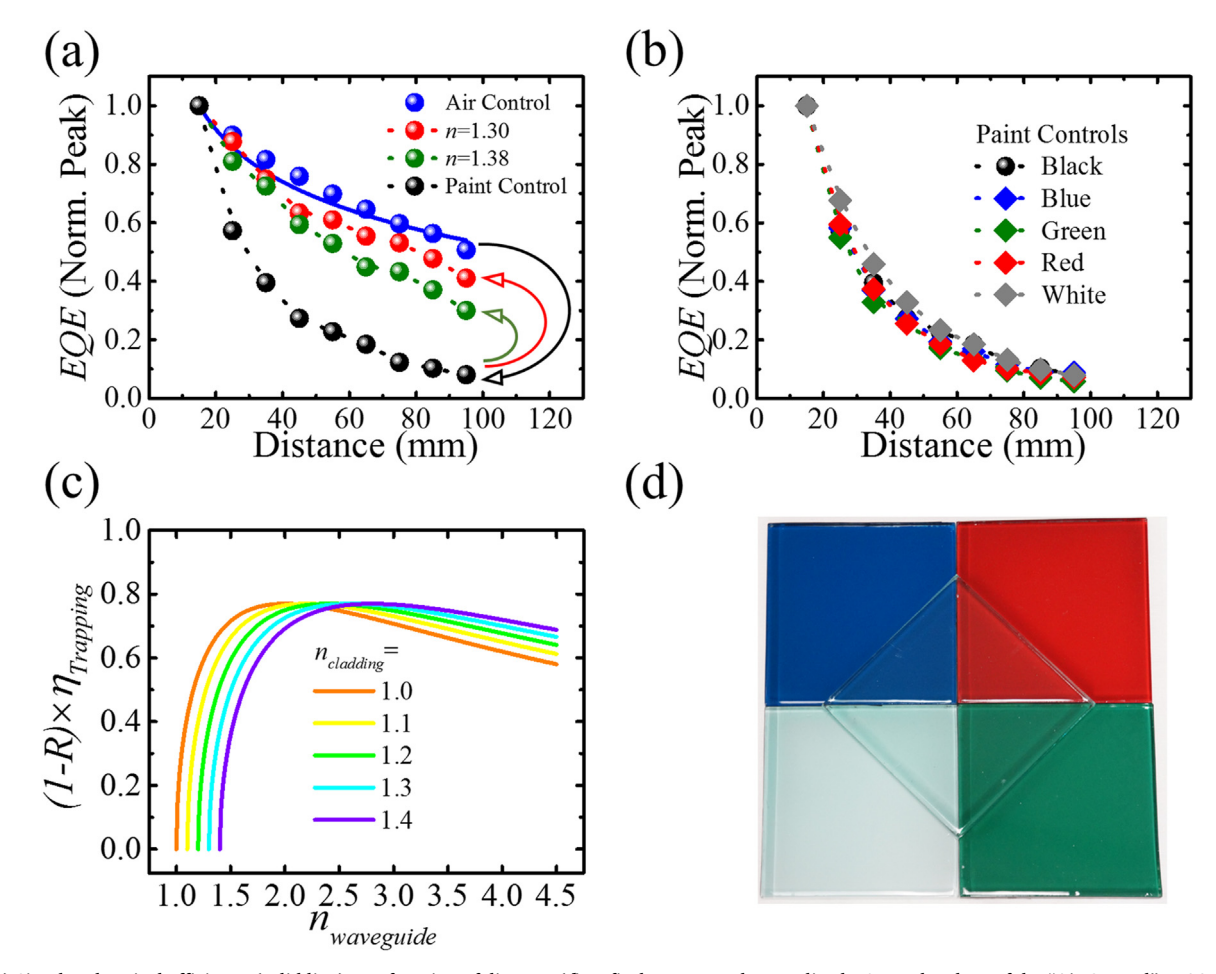


Fig. 4. (a) Simulated optical efficiency (solid line) as a function of distance (d) to fit the measured normalized EQE peak values of the "Air Control" TLSC system. The measured normalized EQE peak values of other TLSC systems including "n = 1.30", "n = 1.38" and "Paint Control" are also plotted for comparison. (b) The measured normalized EQE peak values of colored (black, blue, green, red and white) "Paint Control" TLSC systems. (c) Product of the reflection and trapping efficiencies $((1-R_f)\cdot\eta_{Trap})$ of simple waveguides for different $n_{cladding}$ (1.0–1.4) scenarios as a function of $n_{waveguide}$. In all cases the maximum product is 0.77. (d) A picture of four colored "Paint Control" TLSCs with an "Air Control" TLSC on top, this picture also shows the dye/polymer composite layers largely do not impact the fidelity of the original aesthetic quality of the surfaces underneath.

decay trends compared to the black "Paint Control" in Fig. 4a since absorption and scattering losses are effectively equivalent.

With the low refractive index film inserted between the waveguide and the paint, the *EQE* roll-off is mitigated substantially for both "n=1.30" and "n=1.38". For "n=1.30", the decay is within 80–85% of the "Air control" which indicates that TIR within the waveguide is essentially fully restored. Integration of lower index could further enhance the refractive index contrast between the waveguide and the its cladding and thus reduce this loss to regain the last 15–20%.

For polymers, there are several major methods to reduce the refractive index including chemical modifications and creating nanoporosity (air-gaps) in the films [44]. Incorporating fluorinated functional groups into the main chains or side chains of the polymer structures can be an effective strategy where fluorine atoms can effectively reduce the dipole moment by localizing the electron density in C-F σ bond and thereby reducing the total molecular polarizability that is tied to the polarizability [45,46]. Utilizing this approach, indices in the range of 1.1–1.3 have been demonstrated [45,46].

As an alternative to low-index polymer layers, inorganic optical cladding can be deposited as an interlayer. For example, the refractive indices of MgF₂, CaF₂ and SiO₂ dense coating films are $n_{MgF_2} = 1.39$, $n_{CaF_2} = 1.44$ and $n_{SiO_2} = 1.46$, and they are among the materials with the lowest refractive index values [47,48]. Increasing the porosity volume fraction of these materials in nanoscale can further reduce the refractive index to < 1.1, and can be obtained with glancing angle deposition

[47-54].

While porous polymer and inorganic films have shown quite low refraction indices, it is still difficult to synthesize mechanically robust layers with minimal haze for n < 1.3 for practical applications. For example, porous structures typically have limited mechanical stability and can become collapsed with excess pressure. Additionally, nanoporous structures can also create additional light scattering which is as detrimental for light trapping as the underlying surface [44,48]. Nonetheless, further enhancements in the waveguide could be achieved with higher complexity optical designs such as distributed Bragg reflectors with tunable stop bands matching the luminescent wavelength range of the luminophores but with greater impact on the color coordinates that vary with angle [2,6,55–57].

To further approach the scaling of the air TLSC devices, it is possible to replace the current waveguide with higher refractive index material $(n_{waveguide}>1.5)$. The optimum of the product of the reflection and trapping efficiencies $((1-R_f)\cdot\eta_{Trap})$ of simple waveguides for different $n_{cladding}$ (1.0–1.4) scenarios as a function of $n_{waveguide}$ is plotted in Fig. 4c. With the higher $n_{cladding}$ provided, the higher $n_{waveguide}$ is required to obtain the maximum product ~ 0.77 . Polymers are often the most suitable waveguide materials since luminophores can be embedding directly into the waveguide via mixing or coated as a luminophore/matrix film onto a surface. Introduction of aromatic rings, halogen atoms (except for fluorine), and sulfur atoms are the most common ways to adjust the polymer refractive index to ~ 1.70 with good visible

transparency. Polymer materials with refractive index > 1.70 have been developed but are typically much more costly and very few are commercially available. Practically, expanding the polymer refractive indices from 1.30 to 1.70 is wide enough for the purpose of waveguiding enhancement [15,58–63]. For example, if the refractive index of the waveguide is $n_{waveguide} = 1.70$ with a low refractive index film cladding of n = 1.30 coated on the backside then η_{Trap} can reach 64.5%, which is very close to the "Air Control" scenario of 74.5%.

The strategy of adjusting the refractive index of different layers in TLSC can also be applied to 1) colorful LSC system when the LSC devices are integrated onto the areas where the aesthetic quality are not a concern and which give more freedom in the luminophore selection; 2) insertion between multijunction LSCs as an interlayer to separate and protect the luminescent flux from each subpanel being reabsorbed by the lower bandgap luminophore; 3) integration onto the transparent surfaces where the glass does not have sufficient transparency in the infrared spectrum; 4) incorporation of the low refractive index layer along with other flexible components (waveguide, luminophore layer and PV), resulting in a mechanically flexible LSC or TLSC devices that can be more readily integrated onto curved surfaces. Finally, it should be noted that while the goal of this work is to demonstrate the optical design which enables LSC application in these aforementioned areas, improvements in the PCE baseline by increasing the cyanine quantum yield as well as reabsorption loss have been published elsewhere [64].

5. Conclusions

In conclusion, we have shown that integrating TLSCs onto to highly absorptive and colorful painted surfaces results in nearly 80% drop in performance. To overcome this deployment limitation we have designed NIR harvesting visibly transparent LSC device that can be seamlessly integrated onto arbitrary surfaces. This is achieved by deploying a thin, low refractive index layer between the backside solid surface and the TLSC waveguide. Photovoltaic characteristic shows that the power lost to scattering or absorption of painted surfaces is notably restored with the aid of this low refractive index layer. The waveguide sheet coated with such low refractive index film show AVTs > 90% and CRIs > 99 so that these low refractive index films add very little visual impact to the overall aesthetic quality of the TLSC system. Moreover, the scalability is expected to be significantly improved while still retaining much of their photovoltaic performance. This work provides a simple and cost-effective optical design to make TLSCs deployable on any surface without visual impact on the surface underneath, further accelerating the potential for these clean, low-cost solar technologies.

Acknowledgments

The authors gratefully acknowledge support from the National Science Foundation under grant CBET-1702591.

References

- R.R. Lunt, T.P. Osedach, P.R. Brown, J.A. Rowehl, V. Bulović, Practical roadmap and limits to nanostructured photovoltaics, Adv. Mater. 23 (2011) 5712–5727, https://doi.org/10.1002/adma.201103404.
- [2] R.R. Lunt, Theoretical limits for visibly transparent photovoltaics, Appl. Phys. Lett. 101 (2012), https://doi.org/10.1063/1.4738896.
- [3] C.J. Traverse, R. Pandey, M.C. Barr, R.R. Lunt, Emergence of highly transparent photovoltaics for distributed applications, Nat. Energy 2 (2017) 849–860, https://doi.org/10.1038/s41560-017-0016-9.
- [4] R.R. Lunt, V. Bulovic, Transparent, near-infrared organic photovoltaic solar cells for window and energy-scavenging applications, Appl. Phys. Lett. 98 (2011) 3–5, https://doi.org/10.1063/1.3567516.
- [5] M.G. Debije, P.P.C. Verbunt, Thirty years of luminescent solar concentrator research: solar energy for the built environment, Adv. Energy Mater. 2 (2012) 12–35, https://doi.org/10.1002/aenm.201100554.
- [6] C. Yang, R.R. Lunt, Limits of visibly transparent luminescent solar concentrators, Adv. Opt. Mater. 5 (2017) 1600851, https://doi.org/10.1002/adom.201600851.
- [7] Y. Zhao, G.A. Meek, B.G. Levine, R.R. Lunt, Near-infrared harvesting transparent luminescent solar concentrators, Adv. Opt. Mater. 2 (2014) 606–611, https://doi.

- org/10.1002/adom.201400103.
- [8] Y. Zhao, R.R. Lunt, Transparent luminescent solar concentrators for large-area solar windows enabled by massive stokes-shift nanocluster phosphors, Adv. Energy Mater. 3 (2013) 1143–1148, https://doi.org/10.1002/aenm.201300173.
- [9] M. Zhu, X. Peng, Z. Wang, Z. Bai, B. Chen, Y. Wang, H. Hao, Z. Shao, H. Zhong, Highly transparent and colour-tunable composite films with increased quantum dot loading, J. Mater. Chem. C 2 (2014) 10031–10036, https://doi.org/10.1039/ C4TC01768D.
- [10] Y. El Mouedden, B. Ding, Q. Song, G. Li, K. Alameh, Encapsulation of tandem organic luminescence solar concentrator with optically transparent triple layers of SiO₂/Epoxy/SiO₂, IEEE J. Sel. Top. Quantum Electron. 22 (2016) 82–87, https://doi.org/10.1109/JSTQE.2015.2444593.
- [11] P.S. Kuttipillai, Y. Zhao, C.J. Traverse, R.J. Staples, B.G. Levine, R.R. Lunt, Phosphorescent nanocluster light-emitting diodes, Adv. Mater. 28 (2016) 320–326, https://doi.org/10.1002/adma.201504548.
- [12] T. Yanai, D.P. Tew, N.C. Handy, A new hybrid exchange-correlation functional using the Coulomb-attenuating method (CAM-B3LYP), Chem. Phys. Lett. 393 (2004) 51–57, https://doi.org/10.1016/j.cplett.2004.06.011.
- [13] S.F.H. Correia, P.P. Lima, P.S. André, M.R.S. Ferreira, L.A.D. Carlos, High-efficiency luminescent solar concentrators for flexible waveguiding photovoltaics, Sol. Energy Mater. Sol. Cells 138 (2015) 51–57, https://doi.org/10.1016/j.solmat.2015.02.032.
- [14] J. Yoon, L. Li, A.V. Semichaevsky, J.H. Ryu, H.T. Johnson, R.G. Nuzzo, J.A. Rogers, Flexible concentrator photovoltaics based on microscale silicon solar cells embedded in luminescent waveguides, Nat. Commun. 2 (2011) 343, https://doi.org/ 10.1038/ncomms1318.
- [15] R. Okutsu, Y. Suzuki, S. Ando, M. Ueda, Poly(thioether sulfone) with High Refractive Index and High Abbe's Number, Macromolecules 41 (2008) 6165–6168, https://doi.org/10.1021/ma800797p.
- [16] H. Li, K. Wu, J. Lim, H.-J. Song, V.I. Klimov, Doctor-blade deposition of quantum dots onto standard window glass for low-loss large-area luminescent solar concentrators, Nat. Energy 1 (2016) 16157, https://doi.org/10.1038/nenergy.2016. 157.
- [17] X. Sheng, C. Yu, V. Malyarchuk, Y. Lee, S. Kim, T. Kim, L. Shen, C. Horng, J. Lutz, N.C. Giebink, J. Park, J.A. Rogers, Silicon-based visible-blind ultraviolet detection and imaging using down-shifting luminophores, Adv. Opt. Mater. 2 (2014) 314–319. https://doi.org/10.1002/adom.201300475.
- [18] J. Zhang, P.D. Badger, S.J. Geib, S. Petoud, Sensitization of near-infrared-emitting lanthanide cations in solution by tropolonate ligands, Angew. Chem. Int. Ed. 44 (2005) 2508–2512, https://doi.org/10.1002/anie.200463081.
- [19] C.R. Ronda, T. Jüstel, H. Nikol, Rare earth phosphors: fundamentals and applications, J. Alloy. Compd. 275–277 (1998) 669–676, https://doi.org/10.1016/S0925 8388(98)00416-2.
- [20] S. Saengkerdsub, H.-J. Im, C. Willis, S. Dai, Pechini-type in-situ polymerizable complex (IPC) method applied to the synthesis of Y2O3:Ln (Ln = Ce or Eu) nanocrystallites, J. Mater. Chem. 14 (2004) 1207–1211, https://doi.org/10.1039/ B309606H.
- [21] A. Sanguineti, A. Monguzzi, G. Vaccaro, F. Meinardi, E. Ronchi, M. Moret, U. Cosentino, G. Moro, R. Simonutti, M. Mauri, R. Tubino, L. Beverina, NIR emitting ytterbium chelates for colourless luminescent solar concentrators, Phys. Chem. Chem. Phys. 14 (2012) 6452–6455. https://doi.org/10.1039/C2CP40791D.
- [22] L.-N. Sun, J.-B. Yu, H.-J. Zhang, Q.-G. Meng, E. Ma, C.-Y. Peng, K.-Y. Yang, Near-infrared luminescent mesoporous materials covalently bonded with ternary lanthanide [Er(III), Nd(III), Yb(III), Sm(III), Pr(III)] complexes, Microporous Mesoporous Mater. 98 (2007) 156–165, https://doi.org/10.1016/j.micromeso. 2006.09.002.
- [23] R. Reisfeld, Y. Kalisky, Nd3+ and Yb3+ germanate and tellurite glasses for fluorescent solar energy collectors, Chem. Phys. Lett. 80 (1981) 178–183, https://doi.org/10.1016/0009-2614(81)80084-X.
- [24] T. Wang, J. Zhang, W. Ma, Y. Luo, L. Wang, Z. Hu, W. Wu, X. Wang, G. Zou, Q. Zhang, Luminescent solar concentrator employing rare earth complex with zero self-absorption loss, Sol. Energy 85 (2011) 2571–2579, https://doi.org/10.1016/j. solener.2011.07.014.
- [25] D.A. Chengelis, A.M. Yingling, P.D. Badger, C.M. Shade, S. Petoud, Incorporating lanthanide cations with cadmium selenide nanocrystals: a strategy to sensitize and protect Tb(III), J. Am. Chem. Soc. 127 (2005) 16752–16753, https://doi.org/10. 1021/ja0511725.
- [26] M.N. Sokolov, M.A. Mihailov, E.V. Peresypkina, K.A. Brylev, N. Kitamura, V.P. Fedin, Highly luminescent complexes [Mo6X8(n-C3F7COO)6]2- (X = Br, I), Dalton Trans. 40 (2011) 6375–6377, https://doi.org/10.1039/C1DT10376H.
- [27] L.R. Bradshaw, K.E. Knowles, S. McDowall, D.R. Gamelin, Nanocrystals for luminescent solar concentrators, Nano Lett. 15 (2015) 1315–1323, https://doi.org/10.1021/nl504510t.
- [28] A.F. Mansour, H.M.A. Killa, S. Abd El-Wanees, M.Y. El-Sayed, Laser dyes doped with poly(ST-Co-MMA) as fluorescent solar collectors and their field performance, Polym. Test. 24 (2005) 519–525, https://doi.org/10.1016/j.polymertesting.2004. 11.014.
- [29] R. Reisfeld, D. Brusilovsky, M. Eyal, E. Miron, Z. Burstein, J. Ivri, A new solid-state tunable laser in the visible, Chem. Phys. Lett. 160 (1989) 43–44, https://doi.org/ 10.1016/0009-2614(89)87552-9.
- [30] M.G. Debije, P.P.C. Verbunt, P.J. Nadkarni, S. Velate, K. Bhaumik, S. Nedumbamana, B.C. Rowan, B.S. Richards, T.L. Hoeks, Promising fluorescent dye for solar energy conversion based on a perylene perinone, Appl. Opt. 50 (2011) 163–169, https://doi.org/10.1364/AO.50.000163.
- [31] B.A. Swartz, T. Cole, A.H. Zewail, Photon trapping and energy transfer in multipledye plastic matrices: an efficient solar-energy concentrator, Opt. Lett. 1 (1977) 73–75, https://doi.org/10.1364/OL.1.000073.

- [32] R.F. Kubin, A.N. Fletcher, Fluorescence quantum yields of some rhodamine dyes, J. Lumin. 27 (1982) 455–462, https://doi.org/10.1016/0022-2313(82)90045-X.
- [33] W.H. Weber, J. Lambe, Luminescent greenhouse collector for solar radiation, Appl. Opt. 15 (1976) 2299–2300, https://doi.org/10.1364/AO.15.002299.
- [34] M.J. Currie, J.K. Mapel, T.D. Heidel, S. Goffri, M.A. Baldo, High-efficiency organic solar concentrators for photovoltaics, Science (80-.) 321 (2008) 226 (LP-228), http://science.sciencemag.org/content/321/5886/226.abstract.
- [35] H. Zhao, D. Benetti, L. Jin, Y. Zhou, F. Rosei, A. Vomiero, Absorption enhancement in "giant" core/alloyed-shell quantum dots for luminescent solar concentrator, Small (2016) 5354–5365, https://doi.org/10.1002/smll.201600945.
- [36] K.E. Knowles, T.B. Kilburn, D.G. Alzate, S. McDowall, D.R. Gamelin, Bright CuInS2/CdS nanocrystal phosphors for high-gain full-spectrum luminescent solar concentrators, Chem. Commun. 51 (2015) 9129–9132, https://doi.org/10.1039/C5CC02007G
- [37] L.H. Slooff, E.E. Bende, A.R. Burgers, T. Budel, M. Pravettoni, R.P. Kenny, E.D. Dunlop, A. Büchtemann, A luminescent solar concentrator with 7.1% power conversion efficiency, Phys. Status Solidi - Rapid Res. Lett. 2 (2008) 257–259, https://doi.org/10.1002/pssr.200802186.
- [38] I. Coropceanu, M. Bawendi, Core/shell quantum dot based luminescent solar concentrators with reduced reabsorption and enhanced efficiency, Nano Lett. (2014), https://doi.org/10.1021/nl501627e.
- [39] C. Li, W. Chen, D. Wu, D. Quan, Z. Zhou, J. Hao, J. Qin, Y. Li, Z. He, K. Wang, Large stokes shift and high efficiency luminescent solar concentrator incorporated with CuInS2/ZnS quantum dots, Sci. Rep. 5 (2015) 17777, https://doi.org/10.1038/ srep17777.
- [40] Y. Zhou, D. Benetti, Z. Fan, H. Zhao, D. Ma, A.O. Govorov, A. Vomiero, F. Rosei, Near infrared, highly efficient luminescent solar concentrators, Adv. Energy Mater. 6 (2016) 1501913, https://doi.org/10.1002/aenm.201501913.
- [41] J.L. Banal, J.M. White, K.P. Ghiggino, W.W.H. Wong, Concentrating aggregationinduced fluorescence in planar waveguides: a proof-of-principle, Sci. Rep. 4 (2014) 4635, https://doi.org/10.1038/srep04635.
- [42] J.L. Banal, B. Zhang, D.J. Jones, K.P. Ghiggino, W.W.H. Wong, Emissive molecular aggregates and energy migration in luminescent solar concentrators, Acc. Chem. Res. 50 (2017) 49–57, https://doi.org/10.1021/acs.accounts.6b00432.
- [43] J.L. Banal, H. Soleimaninejad, F.M. Jradi, M. Liu, J.M. White, A.W. Blakers, M.W. Cooper, D.J. Jones, K.P. Ghiggino, S.R. Marder, T.A. Smith, W.W.H. Wong, Energy migration in organic solar concentrators with a molecularly insulated perylene diimide, J. Phys. Chem. C 120 (2016) 12952–12958, https://doi.org/10.1021/acs.incc.6b04479.
- [44] S. Walheim, E. Schäffer, J. Mlynek, U. Steiner, Nanophase-separated polymer films as high-performance antireflection coatings, Science (80-.) 283 (1999) 520 (LP-522), https://science.sciencemag.org/content/283/5401/520.abstract.
- [45] S.A. Sydlik, Z. Chen, T.M. Swager, Triptycene polyimides: soluble polymers with high thermal stability and low refractive indices, Macromolecules 44 (2011) 976–980, https://doi.org/10.1021/ma101333p.
- [46] W. Groh, A. Zimmermann, What is the lowest refractive index of an organic polymer? Macromolecules 24 (1991) 6660–6663, https://doi.org/10.1021/ ma00025a016
- [47] E.F. Schubert, J.K. Kim, Low-refractive-index materials: A new class of optical thinfilm materials, in: Proceedings of International Conference Numer. Simul. Optoelectron. Devices, 2007, pp. 1–2 http://dx.doi.org/10.1109/NUSOD.2007.4348994).
- [48] J.-Q. Xi, J.K. Kim, E.F. Schubert, D. Ye, T.-M. Lu, S.-Y. Lin, J.S. Juneja, Very low-refractive-index optical thin films consisting of an array of SiO2 nanorods, Opt. Lett.

- 31 (2006) 601-603, https://doi.org/10.1364/OL.31.000601.
- [49] J.-Q. Xi, M.F. Schubert, J.K. Kim, E.F. Schubert, M. Chen, S.-Y. Lin, W. Liu, J.A. Smart, Optical thin-film materials with low refractive index for broadband elimination of Fresnel reflection, Nat. Photonics 1 (2007) 176, https://doi.org/10. 1038/nphoton.2007.26.
- [50] J.-Q. Xi, J.K. Kim, E.F. Schubert, Silica nanorod-array films with very low refractive indices, Nano Lett. 5 (2005) 1385–1387, https://doi.org/10.1021/nl050698k.
- [51] X. Yan, D.J. Poxson, J. Cho, R.E. Welser, A.K. Sood, J.K. Kim, E.F. Schubert, Enhanced omnidirectional photovoltaic performance of solar cells using multiplediscrete-layer tailored- and low-refractive index anti-reflection coatings, Adv. Funct. Mater. 23 (2012) 583–590, https://doi.org/10.1002/adfm.201201032.
- [52] F. Guillemot, A. Brunet-Bruneau, E. Bourgeat-Lami, T. Gacoin, E. Barthel, J.-P. Boilot, Latex-templated silica films: tailoring porosity to get a stable low-refractive index, Chem. Mater. 22 (2010) 2822–2828, https://doi.org/10.1021/cm90.2754k
- [53] J.-Q. Xi, M. Ojha, W. Cho, J.L. Plawsky, W.N. Gill, T. Gessmann, E.F. Schubert, Omnidirectional reflector using nanoporous SiO2 as a low-refractive-index material, Opt. Lett. 30 (2005) 1518–1520, https://doi.org/10.1364/OL.30.001518.
- [54] P. Falcaro, D. Grosso, H. Amenitsch, P. Innocenzi, Silica orthorhombic Mesostructured films with low refractive index and high thermal stability, J. Phys. Chem. B 108 (2004) 10942–10948, https://doi.org/10.1021/jp037740p.
- [55] M.C. Barr, R.R. Lunt, V. Bulovic, Patent NO. US 20130333755 Al, 2013.
- [56] M.F. Schubert, J.-Q. Xi, J.K. Kim, E.F. Schubert, Distributed Bragg reflector consisting of high- and low-refractive-index thin film layers made of the same material, Appl. Phys. Lett. 90 (2007) 141115, https://doi.org/10.1063/1.2720269.
- [57] L. Xu, Y. Yao, N.D. Bronstein, L. Li, A.P. Alivisatos, R.G. Nuzzo, Enhanced photon collection in luminescent solar concentrators with distributed Bragg reflectors, ACS Photonics 3 (2016) 278–285, https://doi.org/10.1021/acsphotonics.5b00630.
- [58] N.-H. You, T. Higashihara, Y. Oishi, S. Ando, M. Ueda, Highly refractive Poly (phenylene thioether) containing triazine unit, Macromolecules 43 (2010) 4613–4615, https://doi.org/10.1021/ma100448d.
- [59] J. Liu, M. Ueda, High refractive index polymers: fundamental research and practical applications, J. Mater. Chem. 19 (2009) 8907–8919, https://doi.org/10.1039/ B909690F.
- [60] T. Badur, C. Dams, N. Hampp, High refractive index polymers by design, Macromolecules 51 (2018) 4220–4228, https://doi.org/10.1021/acs.macromol. 8b00615.
- [61] J.J. Griebel, S. Namnabat, E.T. Kim, R. Himmelhuber, D.H. Moronta, W.J. Chung, A.G. Simmonds, K.-J. Kim, J. van der Laan, N.A. Nguyen, E.L. Dereniak, M.E. Mackay, K. Char, R.S. Glass, R.A. Norwood, J. Pyun, New infrared transmitting material via inverse vulcanization of elemental sulfur to prepare high refractive index polymers, Adv. Mater. 26 (2014) 3014–3018, https://doi.org/10.1002/adma. 201305607.
- [62] T. Higashihara, M. Ueda, Recent progress in high refractive index polymers, Macromolecules 48 (2015) 1915–1929, https://doi.org/10.1021/ma502569r.
- [63] A. Javadi, A. Shockravi, A. Rafieimanesh, A. Malek, S. Ando, Synthesis and structure–property relationships of novel thiazole-containing poly(amide imide)s with high refractive indices and low birefringences, Polym. Int. 64 (2014) 486–495, https://doi.org/10.1002/pi.4815.
- [64] C. Yang, J. Zhang, W.-T. Peng, W. Sheng, D. Liu, P.S. Kuttipillai, M. Young, M.R. Donahue, B.G. Levine, B. Borhan, R.R. Lunt, Impact of stokes shift on the performance of near-infrared harvesting transparent luminescent solar concentrators, Sci. Rep. 8 (2018) 16359, https://doi.org/10.1038/s41598-018-34442-3.